ELSEVIER

July 1995

Optical Materials 4 (1995) 597–607

OPTICAL Materials

Quantitative analysis of erbium luminescence in $LiYF_4$ doped with low (1.41%) and high (38.5%) Er^{+3} concentrations

M.B. Camargo, L. Gomes, S.P. Morato

Instituto de Pesquisas Energéticas e Nucleares, CNEN/SP, Caixa Postal 11049, Pinheiros, 05422-970 São Paulo, Brazil

Received 2 November 1994; revised version received 4 February 1995

Abstract

The luminescent-channel efficiency for Er^{+3} ions in $LiYF_4:Er^{+3}$ (38.5%) crystal was measured and compared with the case of Er^{+3} as a low-concentration dopant (1.41%) in crystals of $LiYF_4$. The $^4S_{3/2} \rightarrow {}^4I_{13/2}$, $^4I_{15/2}$ luminescent transitions are strongly quenched in the high concentrated system, by two possible cross-relaxation processes involving one phonon absorption, favoring the population of the $^4I_{11/2}$ and $^4I_{13/2}$ levels. A strong quenching of the total Er^{+3} luminescence by approximately 6.8 times was observed in the highly doped system at 300 K. The two middle infrared (mid-IR) $^4I_{11/2} \rightarrow {}^4I_{13/2}$ and $^4I_{13/2} \rightarrow {}^4I_{15/2}$ luminescent transitions were quenched by an attributed energy transfer from the Er^{3+} excited $^4I_{11/2}$ and $^4I_{13/2}$ levels to $Me^{++}(OH^-)_2$ and HCO^- molecules that are present in the host material as impurities.

1. Introduction

To determine if an ion doped material is a good laser candidate, it is important to characterize it regarding its optical properties as function of the luminescent ion concentration, since it is well established that quenching effects are detrimental to the population inversion processes [1]. Particularly to the Holmiun sensitization when erbium ions are working like donors for Ho^{+3} ions excitation for holmiun laser action at 2.1 μm in laser crystals.

The Er^{3+} ion is used as dopant in several laser host materials showing a broad range of luminescent transitions from 0.50 to 3.00 μm [2,3]. Some of these transitions are laser active, i.e.:

0.85 μm ($^4S_{3/2} \rightarrow {}^4I_{13/2}$),

1.23 μm ($^4S_{3/2} \rightarrow {}^4I_{11/2}$),

1.54 μm ($^4I_{13/2} \rightarrow {}^4I_{15/2}$),

1.73 μm ($^4S_{3/2} \rightarrow {}^4I_{9/2}$),

2.74 μm ($^4I_{11/2} \rightarrow {}^4I_{13/2}$).

The most important transition for the Er^{+3} laser sources is the one in the wavelength interval [4] from 2.66 to 3.00 μm, since they overlap strongly with the water absorption and can be transmitted through special optical fibers.

This combination of properties makes them suitable for medical applications. As biological tissues are composed mainly by water, the use of mid-IR lasers will favor a precise cut or evaporation of biological materials via thermal effects without spurious water photodissociation processes that would occur if the laser source were in the UV [2]. Depending on the desired emission line, laser action can be obtained by pumping the material with Xe flash lamps, Ar or Kr lasers, Er: glass lasers or diode lasers.

The laser performance of highly concentrated Er^{+3} materials (up to 100%) is known in some garnets:

SSDI 0925-3467(95)0005-4

YAG [1–4–6], $YAlO_3$ [2,7], YSGG [8], and YGG [6]. Laser action at 2.94 μm in YAG is more efficient when Er^{+3} concentration [4] is higher than 10%.

For pure crystals of $LiErF_4$ (YLF:Er^{+3} at 100%) it was shown that at 300 K only a weak visible luminescence is observed. However, at 77 K, a strong green emission shows up indicating that the $^4S_{3/2}$ level emission is suppressed at high temperatures [9]. Spectroscopical measurements and branching ratios of the Er^{+3}:YLF luminescence at 15 K up to 2.00 μm were performed by Renfro et al. [10] without mentioning the used concentration. Some authors give the ideal concentrations of the Er^{+3} in YLF for laser action such as: 2% for 0.85 μm [11], 6% for 1.73 μm [12], and 15% to 50% for 2.74 μm [11,13]. These results indicate that the Er^{+3} laser wavelengths are somehow dependent upon the concentration, with longer wavelengths being favored by high doping.

Excited state absorption spectroscopy, lifetimes and energy transfer mechanisms of Er^{+3} in YLF were studied by Rubin et al. [14] for concentrations of 1% to 100%. Pulsed laser action at 2.80 μm was obtained with 8% Er^{+3} in YLF crystals at 300 K by InAs diode laser pumping [15]. An Er^{+3} concentration quenching study for the $^4S_{3/2}$ luminescent transition was made for values from 1% to 100% in YLF crystals resulting in an ideal concentration range from 2% to 5% for efficient [16] luminescent transitions $^4S_{3/2}$ to ^4I_J (J= 9/2, 11/2, 13/2, 15/2).

Considering all these results, a systematic approach that would indicate simultaneously the concentration and temperature effects in the Er^{+3} luminescent levels in YLF was still missing. The branching ratios of the several luminescent channels below 1.05 μm as well as the contribution of the integrated emission in the mid-IR was not known so far. In this work we did a quantitative investigation of the efficiency of each luminescent channel of the Er^{+3} ion, exciting the $^4G_{11/2}$ level which is above the fluorescent level $^4S_{3/2}$. Two crystals with 1.42 and 38.5% of Er^{+3} ions in YLF (measured concentrations) were studied and the results compared. This study is an important approach to examine the performance of the Er^{+3} ion as a laser source in crystals which can be subjected to some contaminant impurities during the synthesis and growth processes. From this point of view, this work can provide useful information for the improvement of solid state laser materials.

2. Experiment

The starting materials for the crystal growth were synthesized from ultra pure rare earth oxides utilizing a conventional hydrofluorination procedure. The Er:YLF thus synthesized was zone refined by one pass due to its incongruent melting characteristic and grown by Czochralski's method under argon atmosphere. The Er:YLF boule underwent a thermal treatment prior to the sample preparation, to eliminate stress originated from the growth process. Samples were extracted from the boule after the appropriate choice of a region free of scattering defects. The samples used here were single crystals of YLF:Er^{+3} (1.42%) and YLF:Er^{+3} (38.5%).

From preliminary optical absorption spectra it was chosen the most intense line of the $^4G_{11/2}$ multiplet (0.376 μm) for excitation, because it can populate very efficiently the $^4S_{3/2}$ metastable state, giving a wide survey for the luminescent study. Samples with 2.74 mm of thickness, were placed in a cold finger of a three-windows refrigerator cryostat, which allows luminescence measurements in a wide range of temperatures from 10 to 300 K. The measurements were taken perpendicularly to the excitation geometry as it is seen in Fig. 1, thus minimizing stray light contribution to the detection system. It was kept the same collecting area from the luminescent surface of the samples by using a fixed excitation area and crystal thickness, for quantitative analysis. All the used samples have the c-axis parallel to the excitation surface.

The excitation at the 0.376 μm wavelength was provided by a stabilized 150 W xenon lamp. The detection

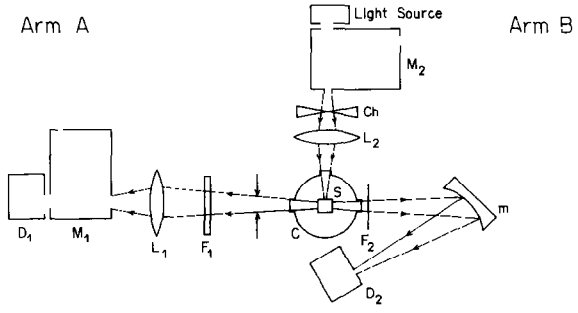

Fig. 1. Experimental setup for the integrated luminescence measurements. D_1, D_2: PMT and InSb detectors, M_1, M_2: monochromators, L_1, L_2 lenses, F_1, F_2: GG 475 (or RG 780) and Si filters, C: refrigerator cryostat, S: sample, Ch: chopper, m: concave aluminum coated mirror with diameter 10 cm (R= 15 cm).

geometry was arranged into two opposite arms as shown in Fig. 1. Emission below 1.05 μm was detected in the arm A utilizing a system composed by a GG 475 (or a RG 780) filter, a Kratos analyzer monochromator (0.25 m) with slits of 1 mm and a S-20 extended (or S-1) photomultiplier (PMT) from EMI. These slits were chosen to match the integration interval (H) to the multiplet width under investigation. In the arm B it was measured and integrated emission above 1.05 μm (mid-IR) utilizing a silicon filter ($T=0.50$ at 1.10 μm), a collecting mirror and a Judson InSb detector (model J-10D) cooled at 77 K. The responsivity of the detectors (in Volt/Watt) were obtained using an electrically calibrated pyroelectric radiometer model RS-5900 from Laser Precision, as a reference.

The transmission band-pass of the analyser monochromator was taken for each luminescent channel in order to correct the values of the luminescence signals. It has always a gaussion shape with a half-width of 12 nm.

The lifetime measurements of the $^4I_{13/2}$ level were obtained from direct measurement of the luminescence decay by pumping the $^2H_{9/2}$ level with a pulsed (10 ns) nitrogen pumped dye laser.

3. Results

The Er^{+3} luminescent channels in YLF crystal were divided as it follows: 0.411; 0.452; 0.502; 0.526; 0.548; 0.665; 0.697; 0.788; 0.847; 0.977 μm and $\lambda \geqslant 1.050$ μm for YLF: (1.42%) and 0.413; 0.452; 0.502; 0.551; 0.667; 0.699; 0.812; 0.851; 0.994 μm and $\lambda \geqslant 1.050$ μm for YLF:Er (38.5%) crystal and they were integrated by a proper detector. The emissions that effectively contribute to the integrated signal for $\lambda \geqslant 1.050$ μm channel was estimated for both crystals by opening completely the slits to 4 mm of the analyzer monochromator in the arm A and using a silicon filter. The results show the following percentual contribution of mid-IR channels for the integrated channel $\lambda \geqslant 1.050$ μm (analyzed in the arm B): $^4I_{11/2} \rightarrow {}^4I_{15/2}$ (1.100 μm) 12.7%; $^4S_{3/2} \rightarrow {}^4I_{11/2}$ (1.23 μm) 4%; $^4I_{13/2} \rightarrow {}^4I_{15/2}$ (1.62 μm) 80%, $^4S_{3/2} \rightarrow {}^4I_{9/2}$ (1.73 μm) 3%; $^4I_{11/2} \rightarrow {}^4I_{13/2}$ (2.74 μm) 0.3% for Er:YLF (1.42%), and 0.2%, 0.02%, 98.5%, 1%, 0.2% for Er:YLF (38.5%), respectively.

The values of integrated luminescent channels were always corrected by a factor (p), which takes into account the transmission band-pass of the analyser monochromator. This factor is defined as the ratio between the corrected signal and the measured one, or:

$$p = \frac{\Sigma_i S_i \Delta(\lambda_i)}{\Sigma_i S_i T_i \Delta(\lambda_i)}, \tag{1}$$

where S_i is the luminescence signal at the wavelength λ_i, T_i is the correspondent transmission of the monochromator and $\Delta(\lambda_i)$ is a constant wavelength interval at λ_i of approximately 2 nm.

One obtains the corrected integrated signal of each luminescent channel by using the expressions:

$$S = \frac{S_I g p f_1}{RT}, \quad \text{for YLF:Er (1.42\%)}, \tag{2}$$

$$S = \frac{S_I g p}{RTf_2}, \quad \text{for YLF:Er (38.5\%)}, \tag{3}$$

where S_I is the measured integrated luminescence signal, g is the ratio between the total solid angle 4π and the one used in Arm A (or B), R is the detector responsivity, f_1 is the ratio of the absorbed power at 300 K to the one at a lower temperature for YLF:Er (1.42%), f_2 is a factor that accounts for the different absorbed power of excitation due to the two erbium concentrations used in the experiment (1.42 and 38.5%) and T is the optical transmission of the filters. For all channels below 0.90 μm, T is 0.95 (GG 475), for all the ones between 0.90 and 1.050 μm, T is 0.66 (RG 780) and $T=0.50$ for $\lambda \geqslant 1.050$ μm (silicon filter).

The estimated f_1 and f_2 values with the temperature are the following

	300 K	206 K	181 K	153 K	100 K	77 K	12 K
f_1	1.00	1.10	1.12	1.14	1.16	1.20	1.46
f_2	1.84	2.02	2.06	2.10	2.14	2.21	2.69

In Tables 1 and 2 are listed the calculated values for the correcting factors (p) for both crystals. In Table 3 are shown the channel band-pass width, the detector responsivities and the optical transmission of the analyser monochromator.

By using Eqs. (2) and (3), one finds the equivalent power of each luminescent channel for both crystals

Table 1
The assumed values for the correcting factors p (defined in the text) used in the quantitative luminescence measurements for YLF:Er (1.42%) crystal as function of the temperature and the wavelength.

λ, (μm)	T						
	12 K	77 K	100 K	153 K	181 K	206 K	300 K
0.411	10.48	10.54	10.99	11.78	12.00	12.53	12.13
0.452	-	11.93	12.63	12.92	12.73	12.23	12.53
0.502	–	39.28	45.36	47.59	48.28	45.90	46.92
0.526	–	–	–	–	46.71	42.71	48.93
0.548	112.59	116.21	119.28	132.70	138.92	143.57	162.72
0.665	6.65	7.23	7.24	8.15	8.40	8.70	10.29
0.697	4.70	5.81	6.54	6.91	7.46	9.19	11.66
0.788	–	–	–	8.18	6.39	6.12	6.78
0.812	–	–	–	–	–	–	–
0.847	4.24	4.02	4.10	4.43	4.42	4.11	4.60
0.977	2.33	2.22	2.40	2.62	2.71	2.82	3.92

and dividing it by the correspondent average photon energy, one gets the number of emitted photons per second for each luminescent channel under continuous pumping with monochromatic light. For the $\lambda \geqslant 1.050$ μm was used an average photon energy of 1.194×10^{-19} joules. These results are shown in Tables 4 and 5 for both crystals at several temperatures. All the losses due to the cryostat windows and lens surfaces were taken into account.

From these results, one can see that the total luminescence of Er^{+3} in the less concentrated crystal does not suffer an accentuated decrease with the temperature increase as was observed in the highly doped one. In the case of the diluted system, the most intense emissions are at 0.548, 0.847 μm and in the mid-IR. Moreover, it is important to note that the 0.977 μm emission is enhanced by a factor of 61 while all others (below 1.05 μm) decreased when the temperature goes from 12 to 300 K.

By comparing the results of both systems, one must conclude that there is a strong quenching of the total Er luminescence in the high concentrated crystal. This means a concentration quenching of 6.8 times at 300 K and 2.2 times at 12 K.

4. Discussion

It is very convenient to define the branching ratio β_i for the ith luminescent channel as $N_i/\Sigma_i N_i$ were N_i is the number of emitted photons per second in this channel and Σ_i is a sum over all the channels. The measured branching ratios β_i for Er^{3+}:YLF were estimated for both crystals and are shown in Tables 6 and 7. For the diluted system (see Table 6), the emission above 1.05 μm corresponds to 5.2% of the total emission when measured at 12 K. For the high concentration sample, this number changes to 16.6%. Increasing the temperature to 300 K there is an effective enhancement of the mid-IR emission for both samples. For the low concentration crystal, the mid-IR luminescence ($\lambda \geqslant 1.05$ μm) is responsible for 14.8% of the total luminescence at 300 K while for the high concentrated crystal its contribution is 80%. The Er^{3+} emission at 0.977 μm ($^4I_{11/2} \rightarrow {}^4I_{15/2}$) [10] was investigated and compared to the 0.847 μm emission. Our conclusion is that the intensity of 0.977 μm emission is one order of magnitude smaller than the 0.847 μm emission. Its contribution is smaller than 3% of the total luminescence in the Er^{3+} (1.41%) YLF at 12 K. On the other hand, that contribution increases to 20% of the total luminescence at 300 K, when all the others decrease.

Considering all these results, one can see immediately that concentration and temperature are both, at the same time, responsible for the emission quenching effects of the transitions $^4S_{3/2} \rightarrow {}^4I_{13/2}$, $^4I_{15/2}$; $^4F_{9/2} \rightarrow {}^{43}I_{15/2}$, and $^2H_{9/2} \rightarrow {}^4I_{11/2}$. At low concentrations (1.42%), one has a very dispersed system with erbium impurities randomly distributed in the lattice, with an average distance of 10.8 Å between Er^{3+} ions. This average distance provides a picture of an isolated ion model. In this case, only 3.7% of the total number of

erbium ions are associated in pairs (two nearest-neighbors Er ions with a minimum approximation of 3.72 Å). The temperature effect observed for this low-concentration system is shown by the decreasing of total luminescence intensity by a factor of 1.29 when going from 12 K to 300 K. In that case, the branching ratios (β_i) of the luminescent channels suffer modifications with temperature as seen in Table 6. This temperature effect is a strong indication that an intracenter nonradiative transitions is occurring in this isolated Er ions system. These mechanisms can be seen in Fig. 2. Particularly, the fact that the radiative $^4S_{3/2} \rightarrow {}^4I_{13/2}$, ($^4I_{15/2}$) transitions are suppressed by 53.5%, (16.6%) at 300 K cannot be explained by all the possible cross-relaxation processes which lead to mid-IR emissions, considering the small fraction of Er^{3+}-pairs in this sample. On the other hand, the multiphonon relaxation mechanisms involving the $^4S_{3/2}$, $^4F_{9/2}$, and $^4I_{11/2}$ levels emitting 9, 8, and 11 phonons, respectively, with an average energy of 331 cm^{-1}, can very efficiently [10] displace the 0.548, 0.665, 0.697 and 0.847 μm emissions to the 0.977 μm and mid-IR region (2.740 μm, $^4I_{11/2} \rightarrow {}^4I_{13/2}$ and 1.540 μm, $^4I_{13/2} \rightarrow {}^4I_{15/2}$).

It is important to note that the branching ratios measured at 12 K, when all the thermally activated processes are improbable, drastically change with the increase of the Er^{3+} concentration to 38.5% (see Tables 6 and 7). This is due to the influence of an Er^{3+} ion on the radiative transitions of the excited partner in the pair. At such level of concentration, one finds 85% of the Er ions associated in pairs, allowing an energy migration through the pairs; e.g. cross-relaxation process including a positive mismatch energy. The same temperature effect is observed in the high concentration sample but much more pronounced. As one can see from the datas presented in Table 5, the 0.851 and 0.551 μm emissions suffer both a strong reduction of 99% instead of 53.5% and 16.6% respectively, observed in the former case. This can be justified by the presence of the quasi-resonant cross-relaxation processes which compete now with the intracenter multiphonon decay, both quenching the luminescent $^4S_{3/2}$ level [17].

Processes numbers 1 and 2 have a negative mismatch energies of 319 and 426 cm^{-1} respectively (see Fig.

Table 3
Assumed values for the channel band-pass width (H), the detectors responsivities (R) and the optical transmission (T_i) of the analyser monochromator

λ, (μm)	H (nm)	R (V/W)	T_i (%)
0.411	24	1.2695×10^9	14.13
0.452	25	1.1908×10^9	9.62
0.502	26	8.4810×10^8	3.56
0.526	24	7.1630×10^8	2.32
0.548	22	5.8440×10^8	1.49
0.665	24	3.8620×10^8	21.96
0.697	24	3.1350×10^8	27.57
0.788	24	3.39×10^7	36.59
0.812	24	2.6×10^6	40.07
0.847	24	1.9×10^6	48.54
0.977	25	1.84×10^5	60.09
(0.994)	25	1.67×10^5	64.63
≥ 1.050	–	4.10×10^2	50.00

Table 2
The assumed values for the correcting factors p (defined in the text) used in the quantitative luminescence measurements for YLF:Er (38.5%) crystal as function of the temperature and the wavelength.

λ, (μm)	T						
	12 K	77 K	100 K	153 K	181 K	206 K	300 K
0.413	9.75	10.54	10.76	10.77	11.03	11.58	13.89
0.452	12.38	13.17	13.37	12.53	13.02	13.07	13.57
0.502	44.68	73.14	73.24	70.28	70.60	61.33	67.73
0.526	–	–	–	–	–	–	–
0.551	100.57	103.74	108.31	118.36	129.39	125.35	143.60
0.667	6.84	7.41	7.65	8.31	9.23	9.59	11.72
0.699	5.17	5.81	5.89	6.92	7.29	7.37	9.89
0.788	–	–	–	–	–	–	–
0.812	–	–	2.86	3.05	2.77	2.96	3.10
0.851	4.41	5.06	5.30	6.21	7.79	8.04	9.80
0.994	2.25	2.14	2.09	2.24	2.26	2.23	2.51

Table 4
The number of the emitted photons per second per luminescent channel ($\times 10^{11}$ photons/sec), at several temperatures for YLF:Er (1.42%) crystal. It is also indicated the correcting factor g for the solid angles used in arms A and B, and the limit of the experimental setup detection. One must consider a typical error of 5% in the values presented in this table.

Transition	λ, (μm)	T						
		12 K	77 K	100 K	153 K	181 K	206 K	300 K
$^2H_{9/2} \rightarrow {}^4I_{15/2}$	0.411	1.73	1.73	1.76	1.84	1.73	1.71	1.03
$^4F_{5/2} \rightarrow {}^4I_{15/2}$	0.452	–	0.064	0.099	0.122	1.011	0.092	0.060
$^4G_{11/2} \rightarrow {}^4I_{13/2}$	0.502	–	0.470	0.730	0.629	0.728	0.788	0.460
$^2H_{11/2} \rightarrow {}^4I_{15/2}$	0.526	–	–	–	–	2.93	5.06	17.3
$^4S_{3/2} \rightarrow {}^4I_{15/2}$	0.548	736	1020	994	1097	907	928	614
$^4F_{9/2} \rightarrow {}^4I_{15/2}$	0.665	126	101	95	92	74	71	50
$^2H_{9/2} \rightarrow {}^4I_{11/2}$	0.697	6.3	8.9	8.7	7.2	6.6	9.5	5.8
$^2H_{11/2} \rightarrow {}^4I_{13/2}$	0.788	–	–	–	1.23	1.63	2.49	10.4
$^4I_{9/2} \rightarrow {}^4I_{15/2}$	0.812	–	–	–	–	–	–	–
$^4S_{3/2} \rightarrow {}^4I_{13/2}$	0.847	3443	3474	3400	2887	2697	2488	1600
$^4I_{11/2} \rightarrow {}^4I_{15/2}$	0.977	11.4	32	57	157	199	273	701
$\lambda \geqslant 1.050$		237	241	277	297	298	370	521
Total		4563	4879	4834	4541	4190	4151	3522

$g = 1790$ for all channels, except for $\lambda \geqslant 1.050$ μm.
$g = 64$ for channels where $\lambda \geqslant 1.050$ μm.
(–) out of the luminescence detectivity limit of 3×10^5 photons/sec.
A typical error of 5% must be considered in all the values presented in the table.

Table 5
The number of the emitted photons per second per luminescent channel ($\times 10^{11}$ photons/sec), at several temperatures for YLF:Er (38.5%) crystal. It is also indicated the correcting factor g for the solid angles used in arms A and B and the limit of the experimental setup detection. One must consider a typical error of 5% in all the values presented in this table.

Transition	λ, (μm)	T						
		12 K	77 K	100 K	153 K	181 K	206 K	300 K
$^2H_{9/2} \rightarrow {}^4I_{15/2}$	0.413	0.55	0.67	0.58	0.29	0.21	0.20	0.075
$^4F_{5/2} \rightarrow {}^4I_{15/2}$	0.452	0.016	0.026	0.063	0.030	0.035	0.025	0.015
$^4G_{11/2} \rightarrow {}^4I_{13/2}$	0.502	0.133	0.245	0.414	0.426	0.473	0.333	0.194
$^2H_{11/2} \rightarrow {}^4I_{15/2}$	0.526	–	–	–	–	–	–	–
$^4S_{3/2} \rightarrow {}^4I_{15/2}$	0.551	339	301	119	20	14	10	3.32
$^4F_{9/2} \rightarrow {}^4I_{15/2}$	0.667	141	88	45	13	8.7	4.9	0.941
$^2H_{9/2} \rightarrow {}^4I_{11/2}$	0.699	5.9	5.6	4.5	3.3	3.5	2.0	0.822
$^2H_{11/2} \rightarrow {}^4I_{13/2}$	0.788	–	–	–	–	–	–	–
$^4I_{9/2} \rightarrow {}^4I_{15/2}$	0.812	–	–	1.72	3.5	3.2	4.3	3.3
$^4S_{3/2} \rightarrow {}^4I_{13/2}$	0.851	1546	1442	661	103	73	45	14
$^4I_{11/2} \rightarrow {}^4I_{15/2}$	0.994	57	128	205	325	290	261	140
$\lambda \geqslant 1.050$		417	588	659	837	774	779	652
Total		2506	2554	1696	1305	1167	1071	815

$g = 1790$ for all the channels, except for $\lambda \geqslant 1.050$ μm.
$g = 64$ for channels where $\lambda \geqslant 1.050$ μm.
(–) out of the luminescence detectivity limit of 3×10^5 photons/sec.
A typical error of 5% must be considered in the values presented in this table.

2), providing an excitation energy migration between donors and acceptors levels.

All the cross-relaxation processes present in the highly concentrated sample are indicated in Fig. 2 with

Table 6
The branching ratios of the luminescent channels β_i, at several temperatures for the YLF:Er (1.42%) crystal. The transitions at 0.411, 0.452 and 0.502 μm are not listed due to their small values ($\leqslant 10^{-4}$).

Transition	λ_i (μm)	T						
		12 K	77 K	100 K	153 K	181 K	206 K	300 K
$^2H_{11/2} \rightarrow {}^4I_{15/2}$	0.526	–	–	–	–	0.0007	0.0012	0.0049
$^4S_{3/2} \rightarrow {}^4I_{15/2}$	0.548	0.161	0.209	0.206	0.242	0.216	0.224	0.174
$^4F_{9/2} \rightarrow {}^4I_{15/2}$	0.665	0.027	0.021	0.019	0.020	0.017	0.017	0.014
$^2H_{9/2} \rightarrow {}^2I_{11/2}$	0.697	0.001	0.002	0.002	0.0016	0.0016	0.002	0.0016
$^2H_{11/2} \rightarrow {}^4I_{13/2}$	0.788	–	–	–	0.0003	0.0004	0.0006	0.0029
$^4S_{3/2} \rightarrow {}^4I_{13/2}$	0.847	0.755	0.712	0.703	0.636	0.644	0.599	0.454
$^4I_{11/2} \rightarrow {}^4I_{15/2}$	0.977	0.002	0.007	0.012	0.035	0.048	0.066	0.199
$\lambda \geqslant 1.050$		0.052	0.049	0.057	0.065	0.071	0.089	0.148

dashed lines. They are written as it follows:

1. $(^4S_{3/2} \rightarrow {}^4I_{9/2})$: $(^4I_{15/2} \rightarrow {}^4I_{13/2}) - 319\ cm^{-1}$,
2. $(^4S_{3/2} \rightarrow {}^4I_{13/2})$: $(^4I_{15/2} \rightarrow {}^4I_{9/2}) - 426\ cm^{-1}$,
3. $(^4F_{9/2} \rightarrow {}^4I_{11/2})$: $(^4I_{15/2} \rightarrow {}^4I_{13/2}) - 1170\ cm^{-1}$,
4. $(^2H_{9/2} \rightarrow {}^4I_{9/2})$: $(^4I_{15/2} \rightarrow {}^4I_{9/2}) - 319\ cm^{-1}$,
5. $(^2H_{11/2} \rightarrow {}^4I_{9/2})$: $(^4I_{15/2} \rightarrow {}^4I_{13/2})$,
6. $(^4F_{9/2} \rightarrow {}^4I_{13/2})$: $(^4I_{15/2} \rightarrow {}^4I_{11/2}) - 1170\ cm^{-1}$.

As a consequence of the processes 3 and 6 between Er^{3+} ions, the emission from the $^4F_{9/2}$ luminescent level is well affected as it is seen by the decreasing intensity of the 0.667 μm luminescence. It has decreased 150 times in the high concentrated crystal at 300 K.

By the same argument, one can explain the effects observed in the 0.413 and 0.699 μm emissions starting from the $^2H_{9/2}$ luminescent level using the cross-relaxation process number 5.

All the cross-relaxation processes here mentioned, provide an excitation energy migration involving the absorption of one (1, 2 and 4) or three (3 and 6) lattice phonons of average [10] energy of 331 cm^{-1}. These mechanisms are thermal activated and should be more effective at room temperature. By these processes, the longest lived [18] levels $^4I_{11/2}$ (4 ms) and $^4I_{13/2}$ (12 ms) are efficiently populated. As a consequence, the two emissions at 2.74 and 1.54 μm should be increased at the expenses of the others.

In this picture, the integrated luminescence of the mid-IR channel ($\lambda \geqslant 1.05$ μm) would be 5.16 times higher than actually it is, in order to preserve the total number of emitted photons per second compared to the Er (1.42%) system at 300 K.

It is important to define now the total luminescence efficiency of both systems as:

Table 7
The branching ratios of the luminescence channels β_i, at several temperatures for the YLF:Er (38.5%) crystal. The transitions at 0.413, 0.452, 0.502 and 0.526 μm are not listed due to their small values ($\leqslant 10^{-4}$).

Transition	λ_i (μm)	T						
		12 K	77 K	100 K	153 K	181 K	206 K	300 K
$^4S_{3/2} \rightarrow {}^4I_{15/2}$	0.551	0.135	0.118	0.070	0.015	0.012	0.0095	0.004
$^4F_{9/2} \rightarrow {}^4I_{15/2}$	0.667	0.056	0.035	0.027	0.0098	0.0074	0.0045	0.0011
$^2H_{9/2} \rightarrow {}^4I_{11/2}$	0.699	0.002	0.002	0.003	0.0025	0.003	0.0019	0.001
$^4I_{9/2} \rightarrow {}^4I_{15/2}$	0.812	–	–	0.001	0.0027	0.0028	0.0041	0.004
$^4S_{3/2} \rightarrow {}^4I_{13/2}$	0.851	0.617	0.564	0.389	0.079	0.0624	0.0426	0.0174
$^4I_{11/2} \rightarrow {}^4I_{15/2}$	0.994	0.023	0.050	0.121	0.249	0.2488	0.2441	0.1713
$\lambda \geqslant 1.050$		0.166	0.230	0.389	0.641	0.6629	0.7274	0.801

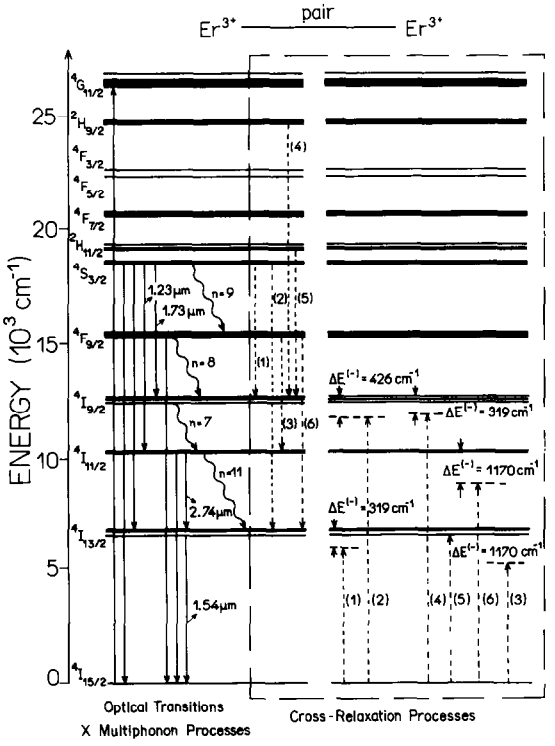

Fig. 2. The Er^{3+} energy levels diagram ion YLF crystal. The optical transitions (solid lines) and the multiphonon decays are indicated in the scheme at left and the ion-ion interaction via cross-relaxation process (numbers 1 to 6) are represented by the dashed lines. (n) is the number of created phonons in the non-radiative relaxations processes. The process (5) is resonant and those ones (1 to 4 and 6) are non-resonants involving a negative mismatch energy $\Delta E^{(-)}$ as it is indicated.

$$\eta_T = \left(\sum_i N_i\right) \Big/ U_0 , \tag{4}$$

where N_i is the number of photons per sec of channel i, the sum (Σ_i) is over all the luminescent channels, and U_0 is the number of excited Er^{3+} ions per sec in the $^4G_{11/2}$ level. U_0 was obtained by using the rate equation of $^4S_{3/2}$ level for the low concentrated system (1.42%). In that case, we can consider that all the excited population from the $^4G_{11/2}$ level is transferred to the $^4S_{3/2}$ level (contributions from highest levels represent less than 1% of total number of emitted photons per sec). In this case, the rate equation for this level is given by the following equation:

$$U_0 = N_1 / \tau_1 , \tag{5}$$

where N_1 is the equilibrium population of $^4S_{3/2}$ level and τ_1 is its total lifetime ($\tau_1 = 0.2$ ms at 300 K [13]).

N_1 was obtained by using the following expression:

$$N_1 = \tau_{r1} \sum_j N_{ij} , \tag{6}$$

where $\tau_{r1} = 0.49$ ms [13] and $i = {}^4S_{3/2}$ level.

The symbol j represents all the luminescent channels starting from $^4S_{3/2}$ level: $j = 0.548, 0.847, 1.230, 1.730$ μm. N_1 was found to be equal to 1.103×10^{11} for Er (1.42%) at 300 K, and $U_0 = 5.51 \times 10^{14}$ s^{-1}.

Using the value of U_0 in Eq. (4) and the number of photons per sec per luminescent channel, presented in the Tables 4 and 5, we could measure the total luminescence efficiency, for both crystals at several temperatures. The results are presented in Table 8. It is important to note that the total luminescence efficiency is drastically reduced with the increase of Er concentration. At 300 K, this efficiency drops to 0.15 as a consequence of the increase of number of Er^{3+}-pairs in the highly concentrated sample.

The increasing of Er^{3+} pairs makes the cross relaxation very efficient and guarantees that each pair have both erbium ions in the two lowest excited states $^4I_{11/2}$ and $^4I_{13/2}$, the longest lived excited states.

An estimate of energy transfer involving erbium ions being one in the $^4I_{13/2}$ and the other in $^4I_{15/2}$ levels was made using the well known Dexter formula [19] for a dipole–dipole interaction. The critical radius (R_c) was estimated for the $^4I_{13/2}$ level using the equation [19]:

Table 8
The total luminescence efficiency (η_T) for both crystals at several temperatures.

Erbium concentration %	T						
	12 K	77 K	100 K	153 K	181 K	206 K	300 K
1.42	0.83	0.88	0.88	0.82	0.76	0.75	0.64
38.5	0.45	0.46	0.31	0.24	0.21	0.19	0.15

$$R_c^6 = \tau(2\pi)^{-4} 6cn^{-2} \int \sigma_a(\lambda)\, \sigma_e(\lambda)\, d\lambda ,$$

where τ is the intra-center lifetime of $^4I_{13/2}$ level (13 ms), n is the index of refraction at 1.54 μm, c is the light velocity, σ_a is the absorption cross section for $^4I_{15/2} \rightarrow {}^4I_{13/2}$ transition, and σ_e is the emission cross section for the $^4I_{13/2} \rightarrow {}^4I_{15/2}$ emission of Erbium ion. The estimated value of R_c is 19.5 Å.

Considering the random distribution of erbium ions in the crystal of YLF:Er (38.5%), we can say that all the erbium ions have another erbium ion, as a nearest closest neighbor, at distances $R \ll R_c$. This means that the energy migration from the $^4I_{13/2}$ level through the crystal lattice due to (Er*–Er) interaction is very efficient. Also, it can be stated that the $^4I_{13/2}$ level is fully efficient in fluorescence, considering its high energy distance of 20 average lattice local phonons to the next lowest level $^4I_{15/2}$. With this argument, one cannot explain the strong quenching observed for the total luminescence, unless one assumes the existence of sinks that are able to trap the migrating energy (from both levels $^4I_{11/2}$ and $^4I_{13/2}$) and dissipate it through the lattice by heating. In order to investigate the presence of any possible molecular impurities which can afford to this observed quenching, it was investigated the infrared absorption in the range of 4000 to 1600 cm^{-1} in both crystals at 300 K. It was seen several absorptions bands at 3610, 2950, 2850, 1735 and 1730 cm^{-1}, which correspond to molecular impurities that are present in tenths of ppm in the YLF:Er (38.5%) crystal. The 3610 cm^{-1} peak is attributed to the $Me^{++}(OH^-)_2$ complexes (Me = Mg, Mn, Ti) [20] and absorptions at 2920 and 2850 cm^{-1} are attributed to HCO^- molecules [21] (as is seen in Fig. 3). There are also some negatively charged molecule (not identified yet) containing CH-bonds absorbing at 2950, 1735 and 1730 cm^{-1}. The fundamental absorption at 3610 cm^{-1} can account for the trapping and absorption of the excitation energy migration from the $^4I_{11/2}$ level in a quasi-resonant transfer process involving a positive mismatch energy of 40 cm^{-1}. The first overtone of the fundamental absorption can also account for the trapping and absorption of excitation from the $^4I_{13/2}$ level with a positive mismatch energy of 727 cm^{-1}.

The nature of this observed quenching process and its correlation with the sink molecules concentration are under investigation.

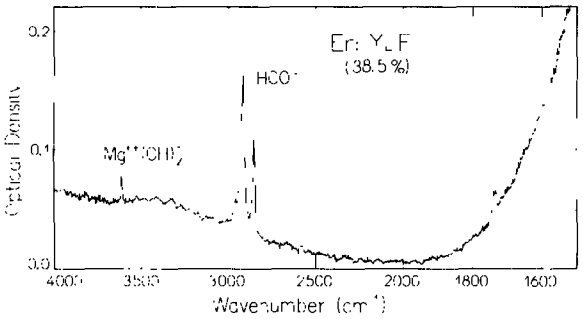

Fig. 3. The infrared spectrum of Er: YLF (38.5%) crystal with 6 mm of thickness, measured at 300 K. Peaks at 1730, 1735 and 2950 cm^{-1} are due to negatively charged molecules containing CH-bonds. Those ones at 2850 and 2920 cm^{-1} are due to HCO^- molecules and the one at 3610 cm^{-1} is due to $Me^{++}(OH^-)_2$ complexes (Me = Mg, Mn, Ti). All these impurities are present in this sample in tenths of ppm.

As far as we know, it is the first time that a quantitative analysis is performed for the total luminescence of Er^{3+} ion in low and high concentrated systems and the possibility of quenching effects.

The measurement of the decay time of $^4I_{13/2}$ level (300 K) for both systems confirm the strong quenching of this fluorescent level in Er:YLF (38.5%). This lifetime is 13 ms for Er (1.42%) and 2.19 ms for (38.5%). It is possible to calculate the probability of the non-radiative transfer (W_{nr}) to the acceptor center (may be the HCO^- molecule), from the measured lifetime (τ) using the expression:

$$W_{nr}(^4I_{13/2}) = \tau^{-1} - \tau^{-1}(\text{intra}) ,$$

where $\tau = 2.19$ ms and $\tau(\text{intra}) = 13$ ms, for the $^4I_{13/2}$ level. The calculated value of W_{nr} was 380 s^{-1}. The lifetime of $^4I_{11/2}$ level should be very short (may be in the scale of μs) and its intensity was very small for Er (38.5%), making its detection not possible.

Another physical parameter (η_p) is very important to define for the high concentrated system. This parameter is the population efficiency of $^4I_{13/2}$ level which can be derived from the rate equation of $^4I_{13/2}$ level, at the equilibrium condition of continuous pumping. This quantity is defined as follows:

$$\eta_p = \frac{\text{population rate}}{\text{excitation rate}} .$$

The excitation rate is $U_0 = 5514.2 \times 10^{11}$ s^{-1} for Er (1.42%) and is ($f_2 U_0$) for Er (38.5%). The population rate is equal to N (1.61 μm), the number of emitted

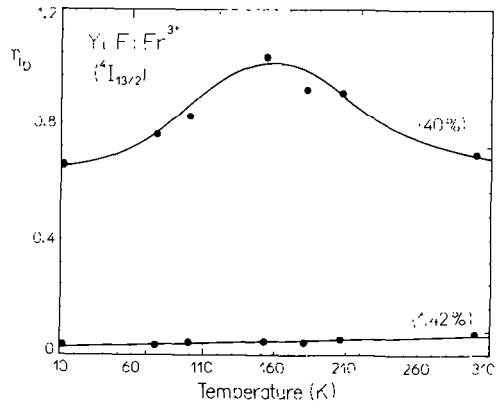

Fig. 4. Temperature dependence of the population efficiency η_p for the $^4I_{13/2}$ fluorescent level in both crystals of YLF with Er (38.5%) and (1.42%), when exciting the $^4I_{15/2} \rightarrow {}^4G_{11/2}$ transition at 0.376 μm. This efficiency has a maximum at 153 K for the high doped crystal.

photons per sec of 1.61 μm channel for Er (1.42%), and is equal to $[f_2\ N(1.61\ \mu m)\ \tau(\text{intra})/\tau]$ for Er (38.5%) crystal. It can be written as

$$\eta_p = N(1.61\ \mu m)/U_0, \quad \text{for Er (1.42\%)},$$

$$\eta_p = [\tau(\text{intra})/\tau][N(1.61\ \mu m)]/U_0, \quad (38.5\%).$$

The values of η_p for $^4I_{13/2}$ level were plotted in Fig. 4. There can be seen that the population efficiency of $^4I_{13/2}$ level in Er:YLF (38.5%) has a strong dependence with the temperature with maximum value of 1.03 at 153 K and a minimum value of 0.65 at 12 K and a value of 0.69 at 300 K. This efficiency quantity is 24 times smaller for Er (1.42%) at 150 K, for an example, in comparison with Er (38.5%).

It is very important to know the population efficiency of $^4I_{13/2}$ level in high-concentrated erbium system from where the excitation can efficiently be transferred to the Ho^{3+} ion exciting it to the $^5I_7$ level and contributing for the holmium laser action at 2.06 μm.

5. Conclusions

Using the total number of emitted photons in both crystals, we got the total luminescence efficiency (η_T) for Er^{3+}.

The strong quenching observed in Er:YLF (38.5%), cannot be explained by a multiphonon nonradiative deexcitation of the level $^4I_{13/2}$ to the $^4I_{15/2}$ ground state. It would be necessary to excite 20 lattice local phonons of 331 cm^{-1} to account for that nonradiative transition, making it impossible in the temperature range investigated.

Using this argument, the unique possible explanation for the observed total luminescence quenching is that one where all the cross-relaxation processes would mainly populate the two longest lived levels $^4I_{11/2}$ and $^4I_{13/2}$ (demonstrated in this case by the values of η_p) favoring a migration of the excitation energy from these levels (the Er distribution shows that the correlation distance R is smaller than R_c (19.5 Å) for the first excited level). These energies can migrate to long distances which finally should be trapped by some modified Erbium ion by the presence of a nearby acceptor molecule which can absorb the excitation, dissipating it in the lattice by phonons creation.

It is important to note that these molecular impurities must not be present in a highly doped laser crystals containing rare-earth (RE^{3+}) ions which emit in this wavelength range, as erbium.

Acknowledgements

The authors thank Prof. Arajá Bandeira, responsible for the Radiometry Laboratory at INPE (Instituto Nacional de Pesquisas Espaciais), for the calibration of the detectors used in the present work.

The authors are also grateful for the financial support received from National Council of Cientific and Technological Development (CNPq) and Assistance Foundation for Research of the State of São Paulo (FAPESP) to develop this work.

References

[1] A.A. Kaminskii, in: Laser Crystals (Springer, Berlin, 1981).
[2] H.P. Weber and W. Luthy, in: Tunable Solid State Lasers II, Springer Series in Optical Sciences 52 (Springer, Berlin, 1986).
[3] S.A. Pollack, D.B. Chang and M. Birnbaum, Appl. Phys. Lett. 54 (1989) 869.
[4] W.Q. Shi, M. Bass and M. Birnbaum, J. Opt. Soc. Am. B 7 (1990) 1456.
[5] A. Charlton, M.R. Dickinson and T.A. King, J. Modern Optics 36 (1989) 1393.
[6] H. Stange, K. Petermann, G. Huber and E.W. Duczynski, Appl. Phys. B 49 (1989) 269.

[7] H. Zbinden, W. Luthy and H.P. Weber, Appl. Phys. Lett. A 52 (1991) 100.
[8] J. Breguet, A.F. Umyskov, W.A.R. Luthy, I.A. Shcherbakov and H.P. Weber, IEEE J. Quantum Electron. 27 (1991) 274.
[9] A.M. Morozov, I.G. Podkolzina, A.M. Tkachuk, V.A. Fedorov and P.P. Feofilov, Opt. Spectrosc. 39 (1975) 338.
[10] G.M. Renfro, J.C. Windscheif and W.A. Sibley, J. Lumin. 22 (1980) 51.
[11] B.M. Antipenko, O.B. Raba, K.B. Seiranyan and L.K. Sukhareva, Sov. J. Quantum Electron. 13 (1983) 1237.
[12] N.P. Barnes, R.E. Allen, L. Esterowitz, E.P. Chicklis, M.G. Knights and H.P. Jensen, IEEE J. Quantum Electron. QE-22 (1986) 237.
[13] F. Auzel, S. Hubert and D. Meichenin, Appl. Phys. Lett. 54 (1989) 691.
[14] J. Rubin, A. Brenier, R. Moncorge and C. Pedrini, J. Lumin. 36 (1986) 39.
[15] G.J. Klintz, R. Allen and L. Esterowitz, Appl. Phys. Lett. 50 (1987) 1553.
[16] A.M. Tkachuk, Opt. Spectrosc. 68 (1990) 775.
[17] A.M. Prokhorov, V.I. Zhekov, T.M. Murina, M.I. Studenikin, V. Lupei, S. Georgescu, A. Lupei and C. Ionescu 33 (1988) 843.
[18] S. Hubert, D.Meichenin, B.W. Zhou and F. Auzel, J. Luminesc. 50 (1991) 7.
[19] D.L. Dexter, J. Chem. Phys. 21 (5) (1953) 836.
[20] T.G. Stoebe, J. Phys. Chem. Sol. 28 (1967) 1375.
[21] Handbook of Chemistry and Physics (The Chemical Rubber Co., 53rd Ed., Ohio, 1972–1973).